

Consistent and Flexible Selectivity Estimation for High-dimensional Data

Yaoshu Wang¹, Chuan Xiao², Jianbin Qin¹, Rui Mao¹, Makoto Onizuka², Wei Wang³, and Rui Zhang⁴

¹Shenzhen Institute of Computing Sciences, ²Osaka University, ³University of New South Wales, ⁴University of Melbourne
{yaoshuw,jqin,mao}@sics.ac.cn,{chuanx,onizuka}@ist.osaka-u.ac.jp,weiw@cse.unsw.edu.au,rui.zhang@unimelb.edu.au

ABSTRACT

Selectivity estimation aims at estimating the number of database objects that satisfy a selection criterion. Answering this problem accurately and efficiently is essential to applications, such as density estimation, outlier detection, query optimization, and data integration. The estimation problem is especially challenging for large-scale high-dimensional data due to the curse of dimensionality, the need to make the estimator consistent (i.e., the selectivity is non-decreasing w.r.t. the threshold), and the large variance of selectivity across different queries. We propose a new deep learning-based model that learns a *query dependent piece-wise linear function* as the estimator. We design a novel model architecture so that the model is flexible to fit any selection criterion. To improve the accuracy for large datasets, we propose to divide the dataset into multiple *disjoint partitions* and build a local model on each of them. We perform experiments on real datasets and show that the proposed model guarantees the consistency and significantly outperforms state-of-the-art models in terms of both accuracy and efficiency.

1 INTRODUCTION

In this paper, we consider the following *selectivity estimation problem* for high-dimensional data: given a query object \mathbf{x} , a distance function d and a distance threshold t , estimate the number of objects \mathbf{o} s in a database that satisfy $d(\mathbf{x}, \mathbf{o}) \leq t$. It is an essential procedure in many applications. For example, it enables us to estimate key distributional statistics, such as local density [36] and outlieriness [4], which are key to density estimation in statistics and density-based outlier detection in data mining. It is also known as the cardinality estimation problem in the database area. Accurate estimation helps to find an optimal query execution plan in databases dealing with high-dimensional data [15]. For example, hands-off entity matching systems [8] extract paths from random forests and take each path (a conjunction of similarity predicates over multiple attributes) as a blocking rule, and efficient blocking can be achieved if we find a good query execution plan.

Selectivity estimation for large-scale high-dimensional data is still an open problem due to the following factors: (i) *Curse of dimensionality*. Many methods that work well on low-dimensional data, such as histograms [17], are intractable when we seek an optimal solution, and they significantly lose accuracy with the increase of dimensionality. (ii) *Consistency requirement*. Given a query object \mathbf{x} , selectivity is non-decreasing with respect to the threshold t . Users may want the estimated selectivity to be consistent and interpretable in applications such as density estimation. This requirement rules out many existing methods. (iii) *Large variance of selectivity*. The selectivity varies across queries and may differ

by several orders of magnitude. A good estimator is supposed to predict accurately for both small and large selectivity values.

To address the above challenges, we propose a novel deep learning-based architecture that guarantees consistency. We holistically approximate the selectivity curve using a continuous piece-wise linear function, consisting of control points that are learned from training data. This function family is flexible in the sense that it can fit the selectivity curve of any input query object closely – e.g., using more control points for the part of the curve where selectivity changes rapidly. Together with a robust loss function, we are able to alleviate the impact of large variance across different queries. To improve the accuracy of estimation on large-scale datasets, we propose a partition-based method to divide the database into multiple *disjoint partitions* and learn a local model on each of them. To ensure consistency, we achieve the monotonicity of estimated selectivity by converting the problem to standard neural network prediction tasks, rather than imposing additional limitations (such as restricting weights to be non-negative [7] or limiting to multilinear functions [9]). To handle the high dimensionality, we incorporate an autoencoder that learns the latent representation of the query object with respect to the whole data distribution. The query object and its latent representation also generate a query-dependent control point model, further improving the quality of the fit to the selectivity curve of the query object. In addition, since update may exist in the database, we propose an incremental learning method to cope with this issue.

We perform experiments on three large-scale real datasets. The experimental results demonstrate that our method outperforms various state-of-the-art models. The improvement of accuracy is significant (by up to 11 times reduction in mean square error) and consistent with respect to datasets, distance functions, and error metrics. The experiments also show that our method is competitive in estimation speed and robust against update in the database.

The rest of the paper is organized as follows. Section 2 reviews related work. Section 3 introduces preliminaries. Section 4 summarizes our observations and ideas. Section 5 presents our model design. Section 6 discusses piece-wise linear functions and the difference between our model and other monotonic methods. We report experimental results in Section 7. Section 8 concludes the paper.

2 RELATED WORK

Traditional Methods. Selectivity estimation has been extensively studied in database systems, where prevalent approaches are based on histograms [17], sampling [37, 39], or sketches [6]. However, few of them are applicable to high-dimensional data due to the curse of dimensionality. Wu *et al.* [38] substantially improved the sample complexity by using LSH as a means to perform important

sampling and get an improved, unbiased estimate of selectivity. This approach is heavily tied to a handful of distance or similarity functions that have known LSH functions. Kernel density estimation (KDE) [15, 24] has been proposed to handle selectivity estimation in metric space. Mattig *et al.* [24] alleviated the curse of dimensionality by focusing on the distribution in metric space. However, strong assumptions are usually imposed on the kernel function (e.g., only diagonal covariance matrix for Gaussian kernels), and one kernel function may be inadequate to model complex distributions in high-dimensional data.

Ordinary Regression Models. Selectivity estimation can be formalized as an ordinary regression problem with query and threshold as input features, if the consistent requirement is not enforced. Traditional learning-based regression models, such as support vector regression, random forest, and XGBoost [5], are difficult to be used for high dimensionality. A recent trend is to use deep learning-based regression models. Vanilla deep regression [21, 32, 33] learns good representations of input patterns. Mixture of expert model (MoE) [29] has a sparsely-gated mixture-of-experts layer that assigns data to proper experts (models) which lead to better generalization. Recursive model index (RMI) [20] is a highly flexible model that can perform regression and can be used to replace the traditional B-tree index in relational databases. Deep learning models have also been used to learn the best join order [22] join size [19], and the selectivity of complex query [23, 31] (just to name a few representative studies). Deep reinforcement learning has been adopted to learn good query plans [26]. Most of the above regression methods (except some tree-based models, e.g., XGBoost and LightGBM) do not guarantee consistency (monotonicity).

Monotonic Models. Isotonic regression [14, 30] fits a free-form monotonic curve to a set of training data. As it is non-parametric, it is not clear how to adapt it to our selectivity estimation problem where the output is only partially monotonic in its input. Min-MaxNet [7] is a monotonic neural network that designs a min-max layer to ensure monotonicity. Training is typically slow as only a small part of the network gets non-zero gradient during back propagation, and its accuracy is not satisfactory [40]. Lattice regression [9, 11, 13, 40] uses (multi-linearly) interpolated look-up table to solve low-dimensional regression problems. By enforcing some constraints on its parameter values, it can guarantee monotonicity. To accommodate high dimensional inputs, Fard *et al.* [9] proposed to build an ensemble of lattice using subsets of input features. The choice of the ensembles is determined either heuristically or randomly. To further increase the modelling power, deep lattice network (DLN) [40] was proposed to interlace non-linear calibration layers and ensemble of lattice layers. Besides, UMNN [35] is an autoregressive flow model which adopts Clenshaw-Curtis quadrature to achieve monotonicity.

3 PRELIMINARIES

3.1 Definitions and Notations

DEFINITION 1 (SELECTIVITY ESTIMATION FOR HIGH DIMENSIONAL DATA). Given a database of multi-dimensional vectors $\mathcal{D} = \{\mathbf{o}_i\}_{i=1}^n$, a distance function $d(\cdot, \cdot)$, a scalar threshold t , and a query object \mathbf{x} , estimate its selectivity in the database, i.e., $|\{\mathbf{o} \mid d(\mathbf{x}, \mathbf{o}) \leq t, \mathbf{o} \in \mathcal{D}\}|$.

While we assume d is a distance function, it is easy to extend it to consider d as a similarity function: we only need to change \leq to \geq in the above definition. In the rest of the paper, when describing our method, we focus on the case when d is a distance function; while we evaluate both distance functions (Euclidean distance) and similarity functions (cosine) in our experiments.

We can view the selectivity (i.e., the ground truth label) y of a query object \mathbf{x} and a threshold t as generated by a function $y = f(\mathbf{x}, t, \mathcal{D})$. We call f the **value function**. Our goal is to estimate $f(\mathbf{x}, t, \mathcal{D})$ using another function $\hat{f}(\mathbf{x}, t, \mathcal{D})$.

One unique requirement of our problem is that the estimator \hat{f} needs to be *consistent*: \hat{f} is consistent if and only if it is *monotonically increasing* in the threshold t ; i.e., $\hat{f}(\mathbf{x}, t', \mathcal{D}) \geq \hat{f}(\mathbf{x}, t, \mathcal{D})$ iff. $t' \geq t$.

4 OBSERVATIONS AND IDEAS

4.1 Observations

When $|\mathcal{D}|$ is large, it is hard to estimate f directly. One of the main challenges is that f may be non-smooth. In the worst case, f is not sufficiently smooth with respect to both input parameters.

- For any \mathbf{y} , there exists a database \mathcal{D} of n objects and a query (\mathbf{x}, t) such that $f(\mathbf{x}, t, \mathcal{D}) = 0$ and $f(\mathbf{x} + \mathbf{y}, t, \mathcal{D}) = n$.
- For any $\epsilon > 0$, There exists a database \mathcal{D} of n objects and a query (\mathbf{x}, t) such that $f(\mathbf{x}, t, \mathcal{D}) = 0$ and $f(\mathbf{x}, t + \epsilon, \mathcal{D}) = n$.

This means any model that directly approximates f is hard.

Our idea to mitigate this issue is to reduce n : instead of estimating one function f , we estimate many functions, such that their output range is mostly a small fraction of n . More specifically, we adopt the following two partitioning methods.

Threshold Partitioning. Given any increasing sequence $[0, t_1, \dots, t_{L+1}]$ such that $t_j > t_i$ for $i < j$, and $t_{L+1} = t$, $t_0 = 0$. We define $\delta t_j = t_j - t_{j-1}$, and $g_j(\mathbf{x}, \delta t_j, \mathcal{D}) = f(\mathbf{x}, t_j, \mathcal{D}) - f(\mathbf{x}, t_{j-1}, \mathcal{D})$. Then $f(\mathbf{x}, t, \mathcal{D}) = \sum_{i=1}^{L+1} g_i(\mathbf{x}, \delta t_i, \mathcal{D})$.

Data Partitioning. We partition the database \mathcal{D} into K disjoint parts, we denote the value function defined on the i -th part as f_i . We have the following observation:

OBSERVATION 1. Given a query (\mathbf{x}, t) , and database \mathcal{D} is partitioned to disjoint $\mathcal{D}_1, \dots, \mathcal{D}_K$, then the final selectivity value will be $f(\mathbf{x}, t, \mathcal{D}) = \sum_{i=1}^K f_i(\mathbf{x}, t, \mathcal{D}_i)$.

In our proposed solution in the next section, we present a model that not only combines both partitioning schemes but also makes the partitions adaptive on the query object and the database. The proposed model guarantees *consistency*, i.e., the learned function is monotonic in the threshold, and provides *flexibility*, i.e., our method is better than previous methods (such as lattice regression) in modelling complex monotonic functions and closely fitting the selectivity curve of any input query.

5 SELECTIVITY ESTIMATOR

5.1 Threshold Partitioning

Our idea is to approximate f using a regression model \hat{f} , which is a continuous piece-wise linear function (denoted by $\hat{f}(\mathbf{x}, t, \mathcal{D}; \Theta)$) with $L + 2$ control (interpolation) points, where L is the number

of control points and 2 refers to the two ends. The parameters in $\hat{f}(\mathbf{x}, t, \mathcal{D}; \Theta)$ are dependent on \mathbf{x} .

Let τ_i denote an control point and p_i denote the estimated selectivity for a query object \mathbf{x} and a threshold τ_i . We consider the family of continuous piece-wise linear function parameterized by $\Theta \stackrel{\text{def}}{=} \{(\tau_i, p_i)\}_{i=0}^{L+1}$.

$$\hat{f}(\mathbf{x}, t, \mathcal{D}; \Theta) = \sum_{i=1}^{L+1} \mathbb{1}[t \in [\tau_{i-1}, \tau_i]] \cdot g_i(\mathbf{x}, t), \quad (1)$$

$$\text{where } g_i(\mathbf{x}, t) = p_{i-1} + \frac{t - \tau_{i-1}}{\tau_i - \tau_{i-1}} \cdot (p_i - p_{i-1}).$$

We assume the maximum threshold we support is t_{\max} . To cover all $t \in [0, t_{\max}]$, we require $\tau_0 = 0$ and $\tau_{L+1} = t_{\max}$. Therefore, we need to learn L τ_i values and $L + 2$ p_i values in Θ . We have the following lemma¹.

LEMMA 1. *Given $p_i \geq p_{i-1}$ for $\forall i, 1 \leq i \leq L + 1$, $\hat{f}(\mathbf{x}, t, \mathcal{D}; \Theta)$ is monotonically increasing with respect to t .*

Estimation Loss. We use the expected loss between f and \hat{f} :

$$J_{\text{est}}(\hat{f}) = \sum_{((\mathbf{x}, t), y) \in \mathcal{T}_{\text{train}}} \ell(f(\mathbf{x}, t, \mathcal{D}), \hat{f}(\mathbf{x}, t, \mathcal{D})). \quad (2)$$

where $\ell(y, \hat{y})$ is a loss function between the actual selectivity y and the current estimate \hat{y} . We choose the Huber loss [16] applied to the logarithmic values of y and \hat{y} . To prevent numeric errors, we also pad the input by a small constant ϵ . Therefore, let $r \stackrel{\text{def}}{=} \log(y + \epsilon) - \log(\hat{y} + \epsilon)$. Then

$$\ell(y, \hat{y}) = \begin{cases} \frac{r^2}{2} & , \text{ if } |r| \leq \delta; \\ \delta(|r| - \frac{\delta}{2}) & , \text{ otherwise.} \end{cases}$$

δ is set to 1.345, the standard recommended value [10]. The reason for designing such a loss function is that the selectivity may differ by several orders of magnitude for different queries. If we use the ℓ_2 loss, it encourages the model to fit large selectivities well, and if we use ℓ_1 loss, it pays more attention to small selectivities. To achieve more robust prediction, we reduce the value range by the logarithm together with the Huber loss.

5.2 Query Dependent Control Points Generation

We need to construct a model to learn the parameters of the model, i.e., L τ_i values, and $L + 2$ p_i values, all in a query dependent way. We learn them separately based on a common enhanced input. We also learn the non-negative increments between consecutive parameters (e.g., τ_i s and p_i) to ensure that they are non-decreasing. In the following, we explain the learning of τ_i s and p_i s, followed by the overall network architecture.

Generating τ_i . Our idea is to learn the increments between τ_i s. Specifically,

$$\tau_i(\mathbf{x}) = \sum_{j=0}^{i-1} \Delta_{\tau}(\mathbf{x})[j],$$

$$\text{where } \Delta_{\tau}(\mathbf{x}) = \text{Norm}_{l_2}(g^{(\tau)}(\mathbf{x})) \cdot t_{\max}.$$

¹Please see Appendix A for proof.

Norm_{l_2} is a normalized squared function and defined as

$$\text{Norm}_{l_2}(\mathbf{t}) = \left[\frac{t_1^2 + \frac{\epsilon}{d}}{\mathbf{t}^T \mathbf{t} + \epsilon}, \dots, \frac{t_d^2 + \frac{\epsilon}{d}}{\mathbf{t}^T \mathbf{t} + \epsilon} \right],$$

where ϵ is a small constant value (to avoid dividing by zero), and d is the dimensionality of \mathbf{t} . The generated model takes \mathbf{x} as input and output L *distinct* threshold points between $(0, t_{\max})$. $g^{(\tau)}$ is implemented by an independent neural network. Then we have a τ vector $\tau = [0; \tau_1; \tau_2; \dots; \tau_L; t_{\max}]$.

One may consider using Softmax(\mathbf{t}), which is widely used as multi-classification and (self-)attention mechanism. We choose Norm_{l_2} rather than Softmax(\mathbf{t}) for the following reasons: First, due to the exponential function in Softmax(\mathbf{t}), a small change of \mathbf{t} might lead to large variations of the output. Second, Softmax aims to highlight important parts rather than partitioning \mathbf{t} , while our goal is to rationally partition the range $[0, \tau_{\max}]$ into several segments such that the piece-wise linear function can fit well.

Generating p_i . We generate $L + 2$ p_i values in a similar fashion, using another neural network to implement $g^{(p)}$.

$$p_i(\mathbf{x}) = \sum_{j=0}^i \Delta_p(\mathbf{x})[j],$$

$$\text{where } \Delta_p(\mathbf{x}) = \text{ReLU}(g^{(p)}(\mathbf{x}))$$

Then we have a \mathbf{p} vector $\mathbf{p} = [p_0; p_1; \dots; p_{L+1}]$. Here, we learn $(L + 1)$ incremental predictions ($p_i - p_{i-1}$) by $g^{(p)}$ instead of directly learning $(L + 2)$ p_i s. In doing so, we do not have to enforce a constraint $p_{i-1} \leq p_i$ for $1 \leq i \leq L + 1$ in the learning process, and thus the learned model can better fit the selectivity curve.

Network Architecture. We illustrate the network architecture of our model in Figure 1.

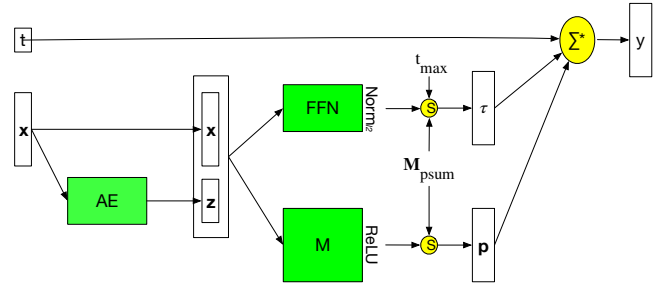


Figure 1: Network architecture.

The input \mathbf{x} is first transformed to $\begin{bmatrix} \mathbf{x} \\ \mathbf{z}_x \end{bmatrix}$, where \mathbf{z}_x is a latent representation of \mathbf{x} obtained by an autoencoder (AE) on the entire dataset. The use of the AE encourages the model to exploit latent data and query distributions in learning piece-wise linear function, and this helps the model generalize to query objects outside the training data. To learn the latent distributions of \mathcal{D} , we pretrain the AE on all the objects in \mathcal{D} , and then continue to train the AE with the queries in the training data.

The enhanced input $\begin{bmatrix} \mathbf{x} \\ \mathbf{z}_x \end{bmatrix}$ is fed into two independent neural networks: a feed-forward network (FFN) and a model M (will be introduced later). Two transformations, denoted by S operators in Figure 1, are needed to separately convert the network output of

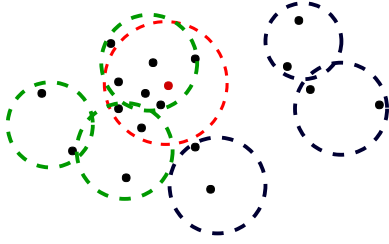


Figure 2: Data partition by cover tree.

FFN and the output of model M to the τ and \mathbf{p} vectors, respectively. They require t_{\max} and a special matrix \mathbf{M}_{psum} which, once multiplied on the right to a vector, perform prefix sum operation on the vector.

$$\mathbf{M}_{\text{psum}} = \begin{bmatrix} 1 & 0 & \dots & 0 \\ 1 & 1 & \dots & 0 \\ \vdots & \vdots & \vdots & \vdots \\ 1 & 1 & \dots & 1 \end{bmatrix}.$$

The output of these networks, together with the threshold t are fed into the operator (denoted by Σ^*) to compute the output of the piece-wise linear function, i.e., the final selectivity estimation.

Design of Model M. To achieve better performance, we learn \mathbf{p} using an encoder-decoder model. In the encoder, a large FFN is used to generate $(L+2)$ embeddings:

$$[\mathbf{h}_0, \mathbf{h}_1, \dots, \mathbf{h}_{L+1}] = \text{FFN}([\mathbf{x}, \mathbf{z}_x]), \quad (3)$$

where \mathbf{h}_i s are high dimensional representations. Here we adopt the $(L+2)$ embeddings, i.e., $\mathbf{h}_0, \dots, \mathbf{h}_{L+1}$, to represent the latent information of \mathbf{p} . In the decoder, we adopt $(L+2)$ linear transformations with ReLU activation function:

$$k_i = \text{ReLU}(\mathbf{w}_i^T \mathbf{h}_i + b_i).$$

Then we have $\mathbf{p} = [k_0, \dots, \sum_{i=0}^{L+1} k_i]$.

The final loss is a linear combination of the estimation loss (Equation (2)) and the loss of the AE for the training data (denoted by J_{AE}):

$$J(\hat{f}) = J_{\text{est}}(\hat{f}) + \lambda \cdot J_{\text{AE}}. \quad (4)$$

5.3 Data Partitioning

To improve the accuracy of estimation on large-scale datasets, we divide the database into multiple disjoint partitions with approximately the same size, and build a local model on each of them. Let $\hat{f}^{(i)}$ denote each local model. We define a global model as $\hat{f}^* = \sum_i \hat{f}^{(i)}$. The final selectivity estimation is $\hat{f}^*(\mathbf{x}, t, \mathcal{D})$.

We have considered several design choices and propose the following configuration that achieves the best empirical performance: (i) partitions obtained by a well-designed partition strategy (introduced later); and (ii) adopting the structure in Figure 1 that all local models share the same transformed input representation, i.e., $\begin{bmatrix} \mathbf{x} \\ \mathbf{z}_x \end{bmatrix}$, but each has its own neural networks to learn the control parameters.

Partitioning Method. We utilize the cover tree data structure [18] to partition \mathcal{D} into several parts. A partition ratio r is predefined such that cover tree will not expand its nodes if the number of data inside is smaller than $r|\mathcal{D}|$. Given a query (\mathbf{x}, t) , the valid region is the circles that intersect the circle with \mathbf{x} as center and t as radius. In Figure 2, \mathbf{x} and t form the red circle range, and data are partitioned into 6 regions. The valid region of (\mathbf{x}, t) is the green circles that intersect the red circle. Albeit imposing constraint, cover tree might still generate too many ball regions, i.e., leaf nodes, which lead to large number of parameters of the model and the difficulty of training. Reducing the number of ball regions is necessary. To solve that, we adopt a merging strategy as follows. First, we still partition \mathcal{D} into K' regions using cover tree. Second, we cluster these regions into K ($K' \leq K$) clusters $\mathcal{D}_1, \dots, \mathcal{D}_K$ using the following greedy strategy: K' regions are sorted in the decreasing order according to the number of their contained data. We begin with K empty clusters. Then we scan each region and assign it into the cluster with the smallest size. All regions that belong to one cluster are merged into one large region. Third, we generate an indicator $f_c : (\mathbf{x}, t) \rightarrow \{0, 1\}^K$, such that $f_c(\mathbf{x}, t)[i] = 1$ if the query (\mathbf{x}, t) has intersection with cluster \mathcal{D}_i . Then we insert the indicator into our model:

$$\hat{f}^*(\mathbf{x}, t, \mathcal{D}) = \sum_{i=0}^K f_c(\mathbf{x}, t)[i] \cdot \hat{f}^{(i)}(\mathbf{x}, t, \mathcal{D}_i).$$

In the applications of selectivity estimation, metric based distance functions (e.g., Euclidean distance) that support triangle inequality are often utilized. Cosine distance can be equivalently converted to Euclidean distance for unit vectors: $\cos(\mathbf{u}, \mathbf{v}) = 1 - \frac{\|\mathbf{u} - \mathbf{v}\|^2}{2}$ for unit vectors \mathbf{u} and \mathbf{v} . So cover tree still works. For distance functions that do not support triangle inequality, we adopt random partitioning instead of cover tree, and modify f_c as $f_c : (\mathbf{x}, t) \rightarrow \mathbf{1}^K$.

Training Procedure. We have several choices on how to train the models from multiple partitions. The default is to directly train the global model \hat{f}^* , with the advantage that no extra work is needed. The other choice is to train each local model independently, using the selectivity computed on the local partition as the training label. We propose yet another choice: we pretrain the local models for T epochs, and then train them jointly. In the joint training stage, we use the following loss function:

$$J_{\text{joint}} = J_{\text{est}}(\hat{f}^{(*)}) + \beta \cdot \sum_i J_{\text{est}}(\hat{f}^{(i)}) + \lambda \cdot J_{\text{AE}}.$$

$f_c(\cdot, \cdot)$ s of all (\mathbf{x}, t) are precomputed before training.

5.4 Dealing With Updates

When the dataset \mathcal{D} is updated with insertion or deletion, we first check whether our model $\hat{f}(\mathbf{x}, t, \mathcal{D})$ is necessary to update. In other words, when minor updates occur and $\hat{f}(\mathbf{x}, t, \mathcal{D})$ is still accurate enough, we ignore them. To check the accuracy of $\hat{f}(\mathbf{x}, t, \mathcal{D})$, we update the labels of all validation data, and re-test the mean absolute error (MAE) of $\hat{f}(\mathbf{x}, t, \mathcal{D})$. If the difference between the original MAE and the new one is no larger than a predefined threshold δ_U , we do not update our model. Otherwise, we adopt incremental learning as follows. First, we update all the labels (ground truth) in the training and the validation data to reflect the update in the

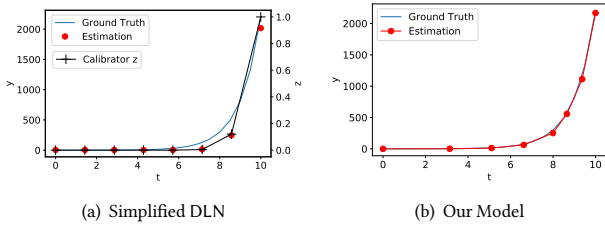


Figure 3: Comparison of using DLN and our model (both with 8 control points) to $y = f(t) = \frac{1}{10} \exp(t)$ for $t \in [0, 10]$.

database. Second, we continue training our model with the updated training data until the validation error (MAE) does not increase in 3 consecutive epochs. Here the training does not start from scratch but from the current model, and we incrementally train our model with all the training data to prevent catastrophic forgetting.

6 DISCUSSION

6.1 Generality of Piece-wise Linear Functions

Piece-wise linear functions are well explored to fit a one-dimensional curve [27]. With enough control points, we can find an optimal set of piece-wise linear functions to fit a one-dimensional curve. The idea of piece-wise linear function is that a small range of input X is highly likely to be linear with output Y . We fully utilize its advantage. For each specific \mathbf{x} , f is only related with t , and can be treated as a one-dimensional curve. To distinguish different \mathbf{x} , we design a deep learning architecture to learn good control points and increments. Our model not only inherits the good performance of piece-wise linear function, but also handles different \mathbf{x} in the high dimension.

6.2 Comparison with Lattice Regression

The lattice regression models are the latest deep learning architectures for monotonic regression. Therefore, we provide a comparison between ours and them applied to selectivity estimation problems. In order to perform an analytical comparison, we make the following simplification. (i) We assume that \mathbf{x} is fixed so it does not affect the estimation. (ii) We consider a *shallow* version of DLN: It consists of one layer of calibrator, followed by a layer of a single lattice. With the above simplification, the DLN model can be analytically represented as:

$$\begin{aligned} \hat{f}_{\text{DLN}}(t) &= h(g(t; \mathbf{w}); \theta_0, \theta_1), \text{ where} \\ g : t \in [0, t_{\max}] &\mapsto z \in [0, 1], \\ h(z; \theta_0, \theta_1) &= (1 - z)\theta_0 + z\theta_1. \end{aligned}$$

Note that lattice regression degenerates to fitting a linear interpolation in a latent space (i.e., z). There is little learning for the function h , as its two parameters θ_0 and θ_1 are determined by the minimum and maximum selectivity values in the training data. Thus, the workhorse of the model is to learn the non-linear mapping of g . This has two inherent limitations:

- The non-linear mapping on t is independent of \mathbf{x} (even though we do not model \mathbf{x} here). Even in the full-fledged DLN model, the

calibration is performed on each input dimension independently. We found that query-dependent fitting of the value function is critical in our problem, as it significantly improves the performance in our empirical evaluation (See Section 7.4).

- The calibrator also uses piece-wise linear functions with K control parameters equivalent to our $(\tau_i, p_i)_{i=1}^K$. However, τ_i s are equally spaced between 0 and t_{\max} , and only p_i s are learnable. This design is not flexible enough for many value functions, e.g., if the function values change rapidly within a small interval, the calibrator won't adaptively allocate more control points within this area.

This effect is best illustrated by a simple example. We use both models with the 8 control points to learn the function $y = f(t) = \frac{1}{10} \exp(t)$, for $t \in [0, 10]^2$. The training data are 80 $(t_i, f(t_i))$ pairs where t_i s are randomly sampled within $[0, 10]$. We plot both models' estimation curves, and their learned control points in Figure 3. Note that the y-axis for the control points for DLN is on the right side of Figure 3(a). We can easily see that: (i) The calibrator virtually determines the estimation as $h()$ degenerates to a simple scaling. (ii) The calibrator's control points are evenly spaced in t , while our model learns to place more controls points in the "interesting area", i.e., where y values change rapidly. This effect will be even more pronounced if we consider the fact that the interesting area varies depending on the query \mathbf{x} . (iii) As a result, our model approximates the value function much better than DLN.

The full-fledged DLN model is too complex to analyze analytically, so we only study it in our empirical evaluation. However, we believe that the above inherent limitations still remain.

6.3 Comparison with Clenshaw-Curtis Quadrature

Clenshaw-Curtis quadrature is able to approximate the integral $\int_0^{\tau_{\max}} \hat{g}(\mathbf{x}, t, \mathcal{D}) dt$, where $\hat{g} = \frac{\partial \hat{f}(\mathbf{x}, t, \mathcal{D})}{\partial t}$ in our problem. UMNN [35] is the latest work that adopts the idea to solve the autoregressive flow problem, and use a neural network to model \hat{g} . In Clenshaw-Curtis scheme [25], the cosine transform of $\hat{g}(\cos\theta)$ is adopted and the discrete finite cosine transform is sampled at *equidistant* points $\theta = \frac{\pi s}{N}$, where $s = 1, \dots, N$, and N is the number of sample points. Compared with our model, it adopts the same integral approximation for different queries, i.e., \mathbf{x} , and ignores that integral points should depend on \mathbf{x} . Instead, our model fully considers this issue, and is more flexible and robust.

7 EVALUATIONS

7.1 Experimental settings

Datasets. We use three embedding datasets³.

- **fasttext** is a pretrained word embedding dataset consisting of 1 million 300-dimensional vectors [1]. We evaluate both cosine and Euclidean (l_2) distances on it as the vectors are not normalized, and denote them as fasttext-cos and fasttext- l_2 , respectively.

²This function has a similar shape with the actual value functions we observed in the experiments (see Figure 4).

³Please see Appendix B for detailed setup, such as data preparation, model settings, and environment.

- **face** is a collection of face embeddings from the face image dataset [2, 12]. We extract 2 million random face images, and obtain their 128-dimensional embedding vectors using the pre-trained faceNet model [28]. We only evaluate cosine distance and dub the setting face-cos, as the vectors are already normalized and selectivity estimation based on Euclidean distance can be reduced to an equivalent estimation problem based on cosine distance.
- **YouTube** is a collection of video records and consists of 0.35 million normalized vectors with 1770 dimension [3]. We only evaluated cosine distance and dub the setting YouTube-cos because its vectors are normalized.

Models. We compare our model with six state-of-the-art models, covering a variety of approaches.

- **KDE** [24] is based on adaptive Kernel density estimation. It only works for metric distance functions. To use KDE with cosine distance, we normalize the dataset to unit vectors and run KDE with Euclidean distance due to the transferability between Euclidean and cosine distance.
- **LightGBM** [34] is based on gradient boosting tree and it supports monotonic regression. Here to fair comparison, we compare with the standard LightGBM and LightGBM-m with monotonic constraint. XGBoost [5] has the same mechanism with LightGBM, so we do not compare it.
- **LSH** [38] is based on importance sampling using locality sensitive hashing that substantially reduces the number of samples required. It only works for the cosine distance due to the use of the SimHash technique. We did not perform the Euclidean distance to cosine conversion as its performance is not competitive.
- Ordinary regression based on deep learning models. We relax the consistency constraint and consider the following deep learning models: **DNN** is a vanilla feed-forward network. **MoE** [29] is a wide Mixture of Expert model with sparse activation. **RMI** [20] is a hierarchical Mixture of Expert model that achieved competitive performance on many traditional database tasks.
- Lattice regression-based models: We adopt the latest model **DLN** [40] in this category.
- Clenshaw-Curtis quadrature-based model: We adopt the latest model **UMNN** [35] in this category.
- Our model is dubbed **SelNet**. We also evaluated two *ablated* model from SelNet.
 - **SelNet_{-ct}** is SelNet *without* partitioning.
 - **SelNet_{-ad-ct}** is SelNet_{-ct} *without* the query dependent control point feature. We disable this feature by feeding a constant vector into the FFN that generates τ .

Metrics. We evaluate Mean Squared Error (MSE), Mean Absolute Error (MAE), and Mean Absolute Percentage Error (MAPE) (see Appendix B.3 for definitions) on both \mathcal{T}_{valid} and \mathcal{T}_{test} .

7.2 Comparison with State-of-the-art Methods

We report the accuracies of all the methods on the three datasets and two distance settings in Table 1–4.

It is clear that our model, SelNet, *robustly* and *significantly* outperforms existing models. It achieves substantial error reduction against the best of the nine state-of-the-art methods, in all three

Model	MSE ($\times 10^5$)		MAE ($\times 10^2$)		MAPE	
	\mathcal{T}_{valid}	\mathcal{T}_{test}	\mathcal{T}_{valid}	\mathcal{T}_{test}	\mathcal{T}_{valid}	\mathcal{T}_{test}
LSH *	70.03	71.45	12.28	13.17	1.38	1.40
KDE *	64.13	64.22	11.71	11.72	1.03	1.01
LightGBM	133.22	130.07	8.44	8.47	0.98	0.97
LightGBM-m	157.25	160.11	9.02	9.08	0.92	0.91
DNN	46.52	46.61	10.23	10.26	0.92	0.93
MoE	57.40	79.83	7.16	7.17	1.35	1.37
RMI	26.73	24.87	8.28	8.25	0.98	0.96
DLN *	56.22	58.57	10.66	10.54	1.07	1.06
UMNN *	23.22	24.69	6.67	6.71	1.21	1.22
SelNet *	4.95	5.08	2.95	2.96	0.63	0.61

Table 1: Accuracy on fasttext-cos. Note that only models marked with a * guarantee consistency.

Model	MSE ($\times 10^5$)		MAE ($\times 10^2$)		MAPE	
	\mathcal{T}_{valid}	\mathcal{T}_{test}	\mathcal{T}_{valid}	\mathcal{T}_{test}	\mathcal{T}_{valid}	\mathcal{T}_{test}
KDE *	24.34	31.40	7.25	8.33	1.51	1.74
LightGBM	164.91	98.77	10.20	9.56	1.25	1.04
LightGBM-m	171.46	101.22	10.13	9.84	1.22	1.20
DNN	46.22	63.54	10.24	11.25	1.28	1.33
MoE	558.56	725.74	8.08	8.31	1.16	1.22
RMI	39.12	40.16	9.19	9.22	1.22	1.24
DLN *	76.04	77.50	11.53	11.56	1.52	1.53
UMNN *	43.11	43.04	8.90	8.89	1.36	1.35
SelNet *	7.65	7.87	3.51	3.56	0.75	0.76

Table 2: Accuracy on fasttext- l_2 .

Model	MSE ($\times 10^5$)		MAE ($\times 10^2$)		MAPE	
	\mathcal{T}_{valid}	\mathcal{T}_{test}	\mathcal{T}_{valid}	\mathcal{T}_{test}	\mathcal{T}_{valid}	\mathcal{T}_{test}
LSH *	277.82	277.35	24.44	25.36	1.25	1.28
KDE *	179.76	182.34	19.65	19.76	0.99	1.01
LightGBM	108.57	101.29	9.76	9.51	0.46	0.45
LightGBM-m	112.44	114.62	10.43	10.46	0.48	0.49
DNN	196.56	110.77	20.05	17.14	0.87	0.89
MoE	15.66	21.25	4.27	4.32	0.29	0.30
RMI	30.72	31.05	7.22	7.24	0.56	0.57
DLN *	126.85	112.36	18.34	18.02	0.98	0.97
UMNN *	16.32	16.75	4.68	4.70	0.38	0.36
SelNet *	5.03	4.96	2.46	2.43	0.22	0.23

Table 3: Accuracy on face-cos.

error metrics on all the settings: the improvement is 2.9–5.2 times reduction in MSE, 1.4–2.4 times reduction in MAE, and 1.4–1.7 times reduction in MAPE.

Among the nine existing methods, the winner really depends on the dataset, the distance function, and the error metric used. For example, MoE performs exceptionally well on face-cos, but it is the worst model on fasttext- l_2 in terms of MSE. UMNN wins on fasttext-cos. Even if we fix an error metric, e.g., MSE, KDE wins on fasttext- l_2 , but far from the winner on the other two settings. These results indicate the challenge of predicting the selectivity accurately and the possible robustness issues with all existing models.

If we only consider models that guarantee consistency (i.e., model names with a * in the tables), the improvement of SelNet is more

Model	MSE ($\times 10^4$)		MAE ($\times 10^2$)		MAPE	
	\mathcal{T}_{valid}	\mathcal{T}_{test}	\mathcal{T}_{valid}	\mathcal{T}_{test}	\mathcal{T}_{valid}	\mathcal{T}_{test}
LSH *	30.25	28.54	1.85	1.83	0.78	0.76
KDE *	28.76	29.25	1.89	1.90	0.74	0.70
LightGBM	39.50	40.11	1.99	2.00	0.51	0.52
LightGBM-m	43.83	54.26	2.12	2.19	0.64	0.65
DNN	25.90	27.76	1.71	1.77	0.49	0.51
MoE	16.13	15.78	1.60	1.59	0.54	0.53
RMI	15.90	17.71	1.58	1.62	0.56	0.55
DLN *	29.25	29.37	1.91	1.92	0.70	0.69
UMNN *	19.04	20.57	1.64	1.69	0.50	0.49
SelNet *	7.21	7.23	1.12	1.13	0.38	0.36

Table 4: Accuracy on YouTube-cos.

LSH *	KDE *	LightGBM	LightGBM-m *	DNN
100	100	86.34	100	78.22
MoE	RMI	DLN *	UMNN *	SelNet *
94.82	90.48	100	100	100

Table 5: Empirical monotonicity (%) on face-cos.

obvious: the improvement is 2.9–6.3 times reduction in MSE, 1.4–3.2 times reduction in MAE, and 1.7–1.9 times reduction in MAPE.

We examine each category of models. We start with the sampling-based method. KDE works better than LSH on all settings. In fact, its performance even outperforms some deep learning regression based methods (e.g., in *fasttext-l₂*). One possible reason is that it focuses on the metric space and escapes the curse of dimensionality.

For tree-based models, LightGBM and LightGBM-m do not perform well. The reason is that they do not learn t well. One interesting observation is that LightGBM-m cannot beat LightGBM in most cases. This indicates that the monotonic constraint, albeit better interpretability, sometimes decreases the performance of regression.

Among the deep learning-based models (including lattice regression and Clenshaw-Curtis quadrature based models), MoE and UMNN slightly outperform others in most cases. For example, in *fasttext-cos* and *fasttext-l₂* datasets, their MAEs are 1.16 and 1.14 times smaller than the best of deep regression models. MoE fails to learn data with large selectivities. In Table 2, its MSE is very large, while its MAE and MAPE are relatively small, which indicates that errors of large selectivities pull up the overall MSE value.

UMNN cannot beat SelNet, e.g., 2.8-5.5 times larger MSE than SelNet, because it does not adopt the query dependent integral and partition strategy. The performance of lattice regression-based model, DLN, is mediocre, even compared with other categories. We believe that the main reason is its inherent limitation to model complex regression problems as in its original design, it considers a narrow class of multi-dimensional monotonic functions, while in our problem the distance function is a one-dimensional (i.e., t) monotonic function.

7.3 Consistency Test

We compute the empirical monotonicity measure [7] and show the results in Table 5. The measure is the percentage of estimated pairs that violate the monotonicity, averaged over 200 queries. For each

Dataset	Model	MSE ($\times 10^4$)		MAE ($\times 10^2$)		MAPE	
		\mathcal{T}_{valid}	\mathcal{T}_{test}	\mathcal{T}_{valid}	\mathcal{T}_{test}	\mathcal{T}_{valid}	\mathcal{T}_{test}
fasttext-cos	SelNet	4.95	5.08	2.95	2.96	0.63	0.61
	SelNet-ct	5.79	5.83	3.12	3.11	0.65	0.63
	SelNet-ad-ct	14.92	14.79	5.22	5.18	1.23	1.22
fasttext-l ₂	SelNet	7.65	7.87	3.51	3.56	0.75	0.76
	SelNet-ct	13.21	12.63	4.33	4.37	0.82	0.81
	SelNet-ad-ct	39.77	39.59	8.77	8.72	2.93	2.90
face-cos	SelNet	5.03	4.96	2.46	2.43	0.22	0.23
	SelNet-ct	5.38	5.31	2.81	2.92	0.23	0.24
	SelNet-ad-ct	16.87	16.02	4.71	4.65	0.38	0.37
YouTube-cos	SelNet	7.21	7.23	1.12	1.13	0.38	0.36
	SelNet-ct	9.04	9.07	1.22	1.20	0.41	0.39
	SelNet-ad-ct	15.27	16.54	1.57	1.59	0.52	0.53

Table 6: Ablation Study

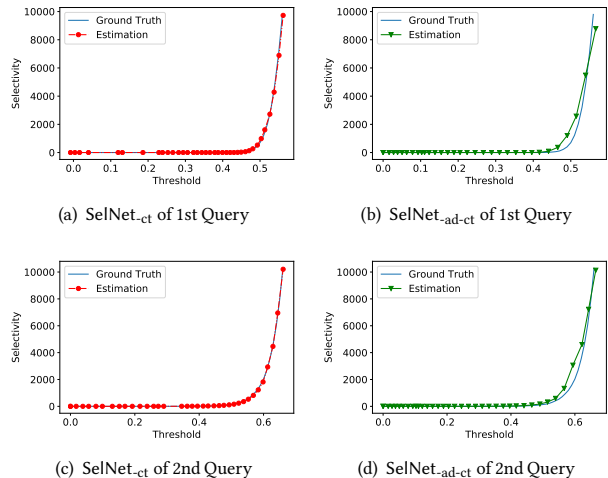


Figure 4: Control points on fasttext-cos.

query, we sampled 100 thresholds, which form $\binom{100}{2}$ pairs. A low score indicates more inconsistent estimates. As expected, models without consistency guarantee cannot produce 100% monotonicity.

7.4 Ablation Study

SelNet-ct v.s. *SelNet*. The main difference between the two models is whether cover tree partition is used. Tables 6 show that the cover tree partition strategy improves the performance. The improvement is especially significant on *fasttext-l₂*, achieving 1.7x and 1.4x reduction in MSE and MAE. This is because the ground truth label values on each model are reduced; this makes it easier to fit our piece-wise linear function with the same number of control parameters, as the value function is less steep.

SelNet-ct v.s. *SelNet-ad-ct*. The main difference between the two models is whether control parameters (τ) are dependent on the query x or not. Table 6 show that this feature has a significant impact on the performance across all settings and all error metrics. For example, on *fasttext-cos*, errors (incl. MSE, MAE, and MAPE) of *SelNet-ct* are nearly 2 times smaller than those of *SelNet-ad-ct*. Similar results can also be found on *fasttext-l₂* and *face-cos*. This is because *SelNet-ct* can use different piece-wise linear functions to approximate the value function for different query objects, as compared with the piece-wise linear functions with the *same set* of

Model	face-cos	fasttext-cos	fasttext- l_2	YouTube-cos
LSH *	1.34	3.65	-	4.95
KDE *	0.85	0.98	0.99	1.13
LightGBM	0.18	0.29	0.28	0.52
LightGBM-m	0.19	0.28	0.28	0.50
DNN	0.03	0.07	0.07	0.16
MoE	0.28	0.39	0.38	0.57
RMI	0.32	0.41	0.40	0.61
DLN *	0.65	0.81	0.83	1.22
UMNN *	0.24	0.37	0.39	0.52
SelNet *	0.20	0.34	0.35	0.51
SelNet- _{ct} *	0.10	0.17	0.16	0.28
SelNet- _{ad-ct} *	0.11	0.16	0.18	0.29

Table 7: Average estimation time (milliseconds).

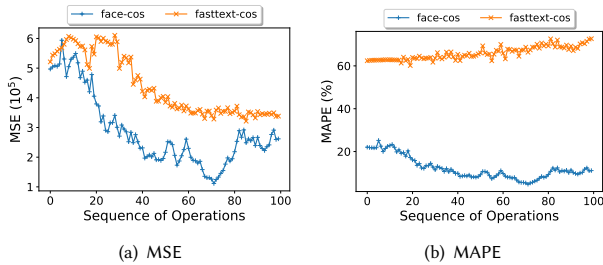


Figure 5: Data update.

τ values in SelNet-_{ad-ct}. To illustrate this point further, we plot the control parameters learned by both models for two random queries in Figure 4. We can see that SelNet-_{ad-ct} used the *same set* of τ values for both queries (i.e., *only* the x -coordinate of the controls points). This is obviously not ideal as a good approximation should devote more points to the thresholds such that the selectivity changes rapidly, and yet such threshold intervals vary from query to query. As a result, SelNet-_{ad-ct} fails to fit the ground truth curve closely especially for quickly changing selectivity values, and results in larger errors across all three metrics.

7.5 Estimation Time

Table 7 shows the estimate time on the testing data. Our model can predict very fast compared with other approaches. Compared with DB approaches, i.e., LSH and KDE, our models have faster prediction time, e.g., at least 2.8 times faster than the best of DB approaches. Among ML models, DNN is the fastest due to its simple model structure. Our models become the runner-up, and their speeds are faster than RMI, MoE DLN and UMNN.

7.6 Evaluation of Data Update

We generate a stream of 100 update operations, each with an insertion or deletion of 5 records on face-cos and fasttext-cos. Figure 5 plots MSE and MAPE changes on a sequence of update operations. The result indicates that incremental learning (Section 5.4) is able to handle updated data. Besides, SelNet only needs 1.5 – 2.0 minutes to perform incremental learning for each update on the two datasets, showcasing its ability to cope with updates.

Error Metric	Number of Control Points			
	10	50	90	130
MSE ($\times 10^5$)	13.06	7.65	7.93	10.47
MAE ($\times 10^2$)	4.85	3.51	3.56	3.92
MAPE	0.87	0.75	0.76	0.79

Table 8: Errors v.s. number of control points on fasttext- l_2 .

Error Metric	Partition Size			
	1	3	6	9
MSE ($\times 10^5$)	13.21	7.65	6.82	6.75
MAE ($\times 10^2$)	4.33	3.51	3.36	3.11
MAPE	0.82	0.75	0.77	0.74
Est. Time (ms)	0.16	0.36	0.79	1.24

Table 9: Errors v.s. partition size on fasttext- l_2 .

Method	CT (3)	RP (3)	KM (3)
MSE ($\times 10^5$)	7.87	8.02	9.14
MAE ($\times 10^2$)	3.56	3.57	3.64
MAPE	0.76	0.78	0.79

Table 10: Errors v.s. partitioning methods on fasttext- l_2 .

7.7 Evaluation of Hyper-parameters

The main hyper-parameters in our models are the number of control points L and partition size K in the cover tree partitioning. Due to the space limitation, we do not show the effect of other hyper-parameters. We make experiments in the validation data as follows. The number of control points is related with the final performance. A small value leads to underfitting towards the curve of thresholds for one specific query, while a large value increases the learning difficulty. Here we fine-tuned L and found that a value of 50 (Table 8) achieves relatively good performance.

We compare SelNet with 1 (equivalent to SelNet-_{ct}), 3, 6, and 9 partitions of fasttext- l_2 in Table 9. The experimental results show that the improvement is small after the partition size reaches a certain value, 6 in fasttext- l_2 . This indicates that a small partition number suffices to achieve good performance. Furthermore, as the partition size increases, estimation time increases. Hence, we use 3 partitions by default in SelNet.

7.8 Evaluation of Partitioning Methods

We compare cover tree partition (CT) with random partition (RP) and k -means partition (KM) in Table 10. KM has the largest errors because it involves imbalance among partitions. CT is slightly better than RP.

7.9 Performance on Thresholds Generated by Beta Distribution

The default training (and validation and test) data generation follows the same way as [24] since such generation method better simulates the realistic workload. Here we consider another type of generation method, where the queries are still randomly sampled from the database, but the thresholds are sampled from a designated distribution. To this end, we use the beta distribution with parameter $\alpha = 3$ and $\beta = 2.5$ for cosine distance. The parameters are

Model	MSE ($\times 10^8$)		MAE ($\times 10^3$)		MAPE	
	\mathcal{T}_{valid}	\mathcal{T}_{test}	\mathcal{T}_{valid}	\mathcal{T}_{test}	\mathcal{T}_{valid}	\mathcal{T}_{test}
LSH *	74.79	69.88	14.55	14.42	1.37	1.35
KDE *	69.53	69.18	14.00	13.90	0.99	1.01
LightGBM	57.44	59.28	12.42	12.48	0.77	0.73
LightGBM-m	68.86	70.11	13.87	13.92	0.74	0.76
DNN	36.10	36.04	10.04	10.03	0.87	0.89
MoE	12.39	11.64	4.33	4.25	1.26	1.20
RMI	20.17	20.23	6.36	6.37	0.65	0.69
DLN *	48.26	47.89	11.50	11.39	1.11	1.13
UMNN *	6.20	6.09	3.58	3.54	0.55	0.52
SelNet *	1.62	1.64	1.74	1.73	0.38	0.38

Table 11: Accuracy on fasttext-cos (thresholds follows the beta distribution $B(3, 2.5)$).

chosen such that the selectivities of many queries changes rapidly within the high probability region of the threshold distribution.

The results are shown in Table 11. Compared with the default training data, all models perform worse, as the range of selectivity values in this workload is larger. Compared with other approaches, SelNet have significant improvement. For example, SelNet has nearly 3.9 times smaller MSE value and 2.1 times MAE when compared with the best previous models (UMNN). Hence, our proposed model demonstrate robustness against training data changes.

8 CONCLUSION

In this paper, we tackle the selectivity estimation problem for high-dimensional data using a novel deep learning architecture. Our method is based on learning query dependent, monotonic continuous piece-wise linear functions. This provides the flexibility of our model to approximate complex functions while still guaranteeing the consistency of estimation. Our extensive experiments demonstrate that the proposed model outperforms previous state-of-the-art methods significantly across a range of settings including datasets, distance functions, and error metrics.

REFERENCES

- [1] <https://fasttext.cc/docs/en/english-vectors.html>.
- [2] <https://www.msceleb.org/>.
- [3] <http://www.cs.tau.ac.il/~wolf/ytfaces/index.html>.
- [4] M. M. Breunig, H. Kriegel, R. T. Ng, and J. Sander. LOF: identifying density-based local outliers. In *SIGMOD*, pages 93–104, 2000.
- [5] T. Chen and C. Guestrin. Xgboost: A scalable tree boosting system. In *KDD*, pages 785–794, 2016.
- [6] G. Cormode, M. N. Garofalakis, P. J. Haas, and C. Jermaine. Synopses for massive data: Samples, histograms, wavelets, sketches. *Foundations and Trends in Databases*, 4(1-3):1–294, 2012.
- [7] H. Daniels and M. Velikova. Monotone and partially monotone neural networks. *IEEE Transactions on Neural Networks*, 21(6):906–917, 2010.
- [8] S. Das, P. S. G. C., A. Doan, J. F. Naughton, G. Krishnan, R. Deep, E. Arcaute, V. Raghavendra, and Y. Park. Falcon: Scaling up hands-off crowdsourced entity matching to build cloud services. In *SIGMOD*, pages 1431–1446, 2017.

- [9] M. M. Fard, K. Canini, A. Cotter, J. Pfeifer, and M. Gupta. Fast and flexible monotonic functions with ensembles of lattices. In *NIPS*, pages 2919–2927, 2016.
- [10] J. Fox. Robust regression: Appendix to an r and s-plus companion to applied regression, 2002.
- [11] E. Garcia and M. Gupta. Lattice regression. In *NIPS*, pages 594–602, 2009.
- [12] Y. Guo, L. Zhang, Y. Hu, X. He, and J. Gao. MS-Celeb-1M: A dataset and benchmark for large scale face recognition. In *ECCV*, 2016.
- [13] M. Gupta, A. Cotter, J. Pfeifer, K. Voevodski, K. Canini, A. Mangylov, W. Moczydlowski, and A. Van Esbroeck. Monotonic calibrated interpolated look-up tables. *The Journal of Machine Learning Research*, 17(1):3790–3836, 2016.
- [14] Q. Han, T. Wang, S. Chatterjee, and R. J. Samworth. Isotonic regression in general dimensions. *arXiv preprint arXiv:1708.09468*, 2017.
- [15] M. Heimel, M. Kiefer, and V. Markl. Self-tuning, GPU-accelerated kernel density models for multidimensional selectivity estimation. In *SIGMOD*, pages 1477–1492, 2015.
- [16] P. J. Huber et al. Robust estimation of a location parameter. *The annals of mathematical statistics*, 35(1):73–101, 1964.
- [17] Y. Ioannidis. The history of histograms (abridged). In *VLDB*, pages 19–30, 2003.
- [18] M. Izbicki and C. R. Shelton. Faster cover trees. In F. R. Bach and D. M. Blei, editors, *ICML*, pages 1162–1170, 2015.
- [19] A. Kipf, T. Kipf, B. Radke, V. Leis, P. A. Boncz, and A. Kemper. Learned cardinalities: Estimating correlated joins with deep learning. In *CIDR*, 2019.
- [20] T. Kraska, A. Beutel, E. H. Chi, J. Dean, and N. Polyzotis. The case for learned index structures. In *SIGMOD*, pages 489–504, 2018.
- [21] S. Lathuilière, P. Mesejo, X. Alameda-Pineda, and R. Horaud. A comprehensive analysis of deep regression. *arXiv preprint arXiv:1803.08450*, 2018.
- [22] R. C. Marcus, P. Negi, H. Mao, C. Zhang, M. Alizadeh, T. Kraska, O. Papaemmanouil, and N. Tatbul. Neo: A learned query optimizer. *PVLDB*, 12(11):1705–1718, 2019.
- [23] R. C. Marcus and O. Papaemmanouil. Plan-structured deep neural network models for query performance prediction. *PVLDB*, 12(11):1733–1746, 2019.
- [24] M. Mattig, T. Fober, C. Beilshmidt, and B. Seeger. Kernel-based cardinality estimation on metric data. In *EDBT*, pages 349–360, 2018.
- [25] M. Novelinkova. Comparison of clenshaw-curtis and gauss quadrature. In *WDS*, volume 11, pages 67–71, 2011.
- [26] J. Ortiz, M. Balazinska, J. Gehrke, and S. S. Keerthi. Learning state representations for query optimization with deep reinforcement learning. In S. Schelter, S. Seufert, and A. Kumar, editors, *DEEM@SIGMOD*, pages 4:1–4:4, 2018.
- [27] L. Prunty. Curve fitting with smooth functions that are piecewise-linear in the limit. *Biometrics*, pages 857–866, 1983.
- [28] F. Schroff, D. Kalenichenko, and J. Philbin. Facenet: A unified embedding for face recognition and clustering. In *CVPR*, pages 815–823, 2015.
- [29] N. Shazeer, A. Mirhoseini, K. Maziarz, A. Davis, Q. Le, G. Hinton, and J. Dean. Outrageously large neural networks: The sparsely-gated mixture-of-experts layer. *arXiv preprint arXiv:1701.06538*, 2017.
- [30] J. Spouge, H. Wan, and W. Wilbur. Least squares isotonic regression in two dimensions. *Journal of Optimization Theory and Applications*, 117(3):585–605, 2003.
- [31] J. Sun and G. Li. An end-to-end learning-based cost estimator. *PVLDB*, 13(3):307–319, 2019.
- [32] Y. Sun, X. Wang, and X. Tang. Deep convolutional network cascade for facial point detection. In *CVPR*, pages 3476–3483, 2013.
- [33] A. Toshev and C. Szegedy. Deeppose: Human pose estimation via deep neural networks. In *CVPR*, pages 1653–1660, 2014.
- [34] D. Wang, Y. Zhang, and Y. Zhao. Lightgbm: An effective mirna classification method in breast cancer patients. In *ICCB*, pages 7–11, 2017.
- [35] A. Wehenkel and G. Louppe. Unconstrained monotonic neural networks. In H. M. Wallach, H. Larochelle, A. Beygelzimer, F. d’Alché-Buc, E. B. Fox, and R. Garnett, editors, *NeurIPS*, pages 1543–1553, 2019.
- [36] K.-Y. Whang, S.-W. Kim, and G. Wiederhold. Dynamic maintenance of data distribution for selectivity estimation. *The VLDB Journal*, 3(1):29–51, 1994.
- [37] W. Wu, J. F. Naughton, and H. Singh. Sampling-based query re-optimization. In *SIGMOD*, pages 1721–1736, 2016.
- [38] X. Wu, M. Charikar, and V. Natthu. Local density estimation in high dimensions. In *ICML*, pages 5293–5301, 2018.
- [39] Y. Wu, D. Agrawal, and A. El Abbadi. Query estimation by adaptive sampling. In *ICDE*, pages 639–648, 2002.
- [40] S. You, D. Ding, K. Canini, J. Pfeifer, and M. Gupta. Deep lattice networks and partial monotonic functions. In *NIPS*, pages 2981–2989, 2017.

A PROOF OF LEMMA 1

PROOF. Assume $t \in [\tau_{i-1}, \tau_i)$, then $t+\epsilon$ is in $[\tau_{i-1}, \tau_i)$ or $[\tau_i, \tau_{i+1})$. In the first case, $\hat{f}(\mathbf{x}, \tau + \epsilon; \Theta) - \hat{f}(\mathbf{x}, \tau; \Theta) = \frac{\epsilon}{\tau_i - \tau_{i-1}} \cdot (p_i - p_{i-1}) \geq 0$. In the second case, $\hat{f}(\mathbf{x}, \tau; \Theta) \leq p_i$ and $\hat{f}(\mathbf{x}, \tau + \epsilon; \Theta) \geq p_i$. Thus, $\hat{f}(\mathbf{x}, t; \Theta)$ is monotonically increasing w.r.t. t . \square

B EXPERIMENT SETUP

B.1 Data Preparation

We randomly sample 0.25 million unique vectors as queries from the dataset \mathcal{D} . In order to generate more representative thresholds for each vector, we follow the approach in [24]: we generate a geometric sequence of w selectivity values in the range $[1, \frac{|\mathcal{D}|}{100}]$, and calculate their corresponding thresholds. The resulting data are randomly split 80:10:10 according to queries into training (\mathcal{T}_{train}), validation (\mathcal{T}_{valid}) and test data (\mathcal{T}_{test}). This ensures that none of the test queries and their thresholds has been seen by the model during the training or validation. We use $w = 40$.

B.2 Model Settings

Hyperparameter and training settings are given below.

- DNN is a vanilla FFN with four hidden layers of sizes 512, 512, 512, and 256.
- MoE consists of 30 expert models, each an FFN with three hidden layers of sizes 512, 512, and 512. We used top-3 experts for the prediction.
- RMI has three levels, with 1, 4, and 8 models, respectively. Each model is a FFN with four hidden layers with sizes 512, 512, 512, and 256.
- DLN is an architecture of six layers: calibrators, linear embedding, calibrators, ensemble of lattices, calibrators, and linear embedding.
- UMNN is a FFN with four hidden layers of sizes 512, 512, 512 and 256 to implement the derivative. $\frac{\partial f(\mathbf{x}, t; \mathcal{D})}{\partial t}$. $f(\mathbf{x}, t, \mathcal{D})$ is computed by Clenshaw-Curtis quadrature with learned derivatives.
- SelNet: We use an FFN with two hidden layers to estimate τ , and an FFN in Equation 3 with four hidden layers to estimate \mathbf{p} . The encoder and decoder of AE are implemented with an FFN with three hidden layers. For face-cos and YouTube-cos datasets, the sizes of the first three (two if not enough) hidden layers of the

three FFNs are 512, and the sizes of all other hidden layers are 256. For fasttext-cos and fasttext- l_2 , the sizes of the first hidden layer of the three FFNs are 1024, and the others remain the same. The number of control parameters L is 50. The (default) partition size is 3. The learning rates of face-cos, fasttext-cos, fasttext- l_2 and YouTube-cos are 0.00003, 0.00002, 0.00002 and 0.00003. $|\mathbf{h}_i|$ ($0 \leq i \leq L + 1$) in model M is 100, and the batch size is 512 for all datasets. We train all models in 1500 epochs, and select the ones with the smallest validation errors. For the training with data partitioning, we use $T = 300$ and $\beta = 0.1$ in our experiments.

For LSH and KDE, we use 2,000 samples to keep the estimation cost reasonable. For all the other models, we train them with the same Huber loss on the logarithm of the ground truth and prediction; all hyper-parameters are fine-tuned according to the validation set. DNN, MoE and RMI cannot directly handle the threshold t . We learn a non-linear transformation of t into an m dimensional embedding vector, i.e., $\mathbf{t} = \text{ReLU}(\mathbf{w}t)$. Then we concatenate it with \mathbf{x} as the input to these models.

B.3 Evaluation Metric

We evaluate Mean Squared Error (MSE), Mean Absolute Error (MAE), and Mean Absolute Percentage Error (MAPE). They are defined as:

$$\text{MSE} = \frac{1}{m} \sum_{i=1}^m (\hat{y}_i - y_i)^2,$$

$$\text{MAE} = \frac{1}{m} \sum_{i=1}^m |\hat{y}_i - y_i|,$$

$$\text{MAPE} = \frac{1}{m} \sum_{i=1}^m \left| \frac{\hat{y}_i - y_i}{y_i} \right|,$$

where y_i is the ground truth value and \hat{y}_i is the estimated value.

B.4 Environment

The experiments were carried out on a server with a Intel Xeon E5-2640 @2.40GHz CPU and 256GB RAM running Ubuntu 16.04.4 LTS. Non-deep models were implemented in C++. Deep models were implemented in python and Tensorflow.

Source codes and datasets are available at <https://github.com/yaoshuwang/SelNet-Estimation>.